How Well Does Water Activity Determine Homogeneous Ice Nucleation Temperature in Aqueous Sulfuric Acid and Ammonium Sulfate Droplets?

BRIAN D. SWANSON

Department of Earth and Space Sciences, University of Washington, Seattle, Washington

(Manuscript received 20 June 2007, in final form 20 August 2008)

ABSTRACT

Frozen fraction measurements made using a droplet free-fall freezing tube apparatus are presented and used, along with other recent laboratory measurements, to evaluate how well both the water activity idea and the translated melting-point curve idea of Koop et al. predict homogeneous freezing-point temperatures for aqueous ammonium sulfate and sulfuric acid solution droplets. The new freezing-point temperature datasets agree with the previous lowest-temperature results for both solutes. The lowest measured freezing-point temperatures for aqueous ammonium sulfate solutions agree with a curve shaped like the translated melting-point curve. However, those for aqueous sulfuric acid solutions are significantly lower than predicted by the translated melting-point curve idea, and a single water activity freezing-point temperature curve does not represent the lowest-temperature freezing-point temperature data for both solutes. A linear extrapolation of the new aqueous sulfuric acid solution freezing data to low temperatures predicts that high critical supersaturations in cloud-free regions of the upper troposphere will occur when homogeneous ice nucleation in an aqueous sulfuric acid aerosol is the primary ice formation mechanism.

1. Introduction

An important uncertainty in climate models is understanding when and where upper-tropospheric ice clouds form. Aqueous solution droplets can freeze at warmer temperatures and lower relative humidity via heterogeneous ice formation processes, and there remains a question about the extent to which the dominant ice formation mechanism below −37°C in the upper troposphere is homogeneous ice nucleation (Sassen and Dodd 1988; Heymsfield and Sabin 1989; DeMott et al. 1994; Jensen et al. 1994; Heymsfield and Miloshevich 1993; DeMott et al. 2003; Abbatt et al. 2006)—particularly for aqueous sulfuric acid and ammonium sulfate droplets (Tabazadeh et al. 1997; Jensen et al. 1998). However, the focus of this paper is the freezing of droplets in which the dominant ice formation mechanism is homogeneous ice nucleation. Over the years, several models, parameterizations, and ideas have been developed to predict the temperature at which homogeneous ice nucleation occurs in aqueous solutions. The most common approach is to use the classical model for homogeneous nucleation, which has been refined in an attempt to predict ice formation in aqueous solution droplets (see Pruppacher and Klett 1997; Jeffery and Austin 1997; Khvorostyanov and Sassen 1998; Khvorostyanov and Curry 2004, and references therein). However, to date this model has limited utility: first, because the model contains only indirect linkage between microscopic ice formation processes and the macroscopic parameters in the model, and second, because the model presently cannot predict ice nucleation temperatures for many aqueous solutions because some of the important parameters in the model (i.e., the interfacial and activation energies) are difficult to measure directly and remain an active subject of research (Baker 1997; DeMott 2002). This fact was recently demonstrated in a careful examination of this theory by Khvorostyanov and Curry (2004), who showed that reasonable fits to freezing-point temperature datasets for aqueous ammonium sulfate and sulfuric acid solutions could only be obtained by tuning the value of the solution–air surface tension.

A second approach, developed over the last few decades, is the so-called melting-to- freezing temperature depression parameterization, based on the fact that

Corresponding author address: Brian D. Swanson, Laucks Foundation Inc., Bellevue, WA 98004.
E-mail: brian@ess.washington.edu

DOI: 10.1175/2008JAS2542.1

both the melting-point and freezing-point temperatures of an aqueous solution decrease with increasing solute concentration. Rasmussen and MacKinzie (1972) began the practice of characterizing freezing temperature depression ($T_f^o - T_f$) by a parameter λ multiplied by the melting-point temperature depression ($T_m^o - T_m$):

$$T_f^o - T_f = \lambda(T_m^o - T_m), \tag{1}$$

where T_f^o and T_m^o are the freezing- and melting-point temperatures of pure water and T_f and T_m are the freezing- and melting-point temperatures of the solution of interest. The parameter λ is an experimentally defined constant (independent of solution concentration), and for many solutions Eq. (1) holds for a range of solution concentration. But to date this approach is also of limited utility: first, because there is still no detailed microphysical explanation for how the processes of melting and freezing are related and second, because this parameterization does not precisely predict ice nucleation temperatures since λ has been shown to vary between $1 < \lambda < 5$ for various solutes (DeMott 2002; Koop 2004; Rasmussen and MacKinzie 1972; Zobrist et al. 2003; Kanno et al. 2007).

A third approach is a relatively new idea published by Koop et al. (2000); it is unique in that it makes a clear prediction for the freezing-point temperature for all aqueous solutions. Koop et al. (2000) showed that when datasets for the freezing-point temperature of numerous aqueous solutions were plotted in terms of water activities a_w[1] rather than solution concentration, these datasets appear to fall on a ''universal'' curve—a curve independent of solute type. I call the idea that freezing-point temperatures for different solutes plotted in terms of water activity fall on a solute-independent universal curve $T_f(a_w)$ the ''water activity'' idea. Furthermore, it is suggested that with a translation in water activity both the melting-point and freezing-point temperature curves can be superimposed such that all data fall along a single similarly shaped temperature versus water activity curve. I call this idea the ''translated melting-point curve'' (TMPC) idea, with the equation for the freezing temperature defined by $a_{w-f}(T)$ being

$$a_{w-f}(T) = a_{w-m}(T) + \Delta a_w, \tag{2}$$

where Δa_w is the shift in water activity. The melting point curve $a_{w-m}(T)$ has not been measured directly at low temperature and is instead parameterized as

$$a_{w-m}(T) = \exp[15.8083 + 25\,301.4\ T^{-1} - 399\,752\ T^{-2} - 5018.85\ \ln(T)/T], \tag{3}$$

in which T is in kelvins and the exponent is a parameterization of the excess Gibbs free energy of water (taken from Johari et al. 1994). This result is consistent with an experimentally determined value at 150 K by Speedy et al. (1996). However, this link between melting and freezing is both intriguing and puzzling.[2]

The strength of the TMPC idea is that it provides a solute-independent prediction for freezing point temperature (which is now dependent only on a_w)—something difficult to obtain from the classical nucleation model or the freezing temperature depression parameterization. The water activity idea is now widely used in cloud models (Kärcher and Lohmann 2002; Haag et al. 2003; Kay et al. 2006; Kärcher et al. 2006) despite the fact that considerable disparity exists between the laboratory datasets for some aqueous solutions. The focus of this paper is to examine the applicability of both the water activity idea and the TMPC idea for two tropospherically important solutions: $(NH_4)_2SO_4$–H_2O and H_2SO_4–H_2O.

2. Apparatus and methodology

A droplet free-fall freezing tube was used to make the measurements reported here. A detailed description of this methodology has been published previously (see Wood et al. 2002; Larson and Swanson 2006), so in this paper I discuss only aspects of the apparatus and methodology that are crucial for evaluating the results presented. The freezing tube consists of a droplet-on-demand droplet generator mounted inside an enclosure that is situated on top of a 50-cm-tall cylindrical freezing tube (see Fig. 1). Outside the freezing tube near the tube top and bottom there are cooling coils through which cryogen is circulated from a cryogenic bath unit. Valves attached to each cooling coil throttle the flow, thereby setting the temperature gradient in the tube. For the results reported here, the top of the freezing tube was

[1] The water activity of a solution is defined as the ratio of the solution's water vapor pressure to the vapor pressure of pure water at the same temperature. Conversion from solution concentration to water activity can be done using aqueous solution models (e.g., Clegg et al. 1998).

[2] The melting of ice is considered the paradigm case of equilibrium first-order phase transitions whereas ice nucleation is considered to be a kinetic nonequilibrium process. A theoretical understanding of how the TMPC idea operates is still lacking (Koop 2004), although exploration of a liquid-only criterion for freezing shows extrema in the compressibility near freezing-point temperatures for some models of water (Baker and Baker 2004).

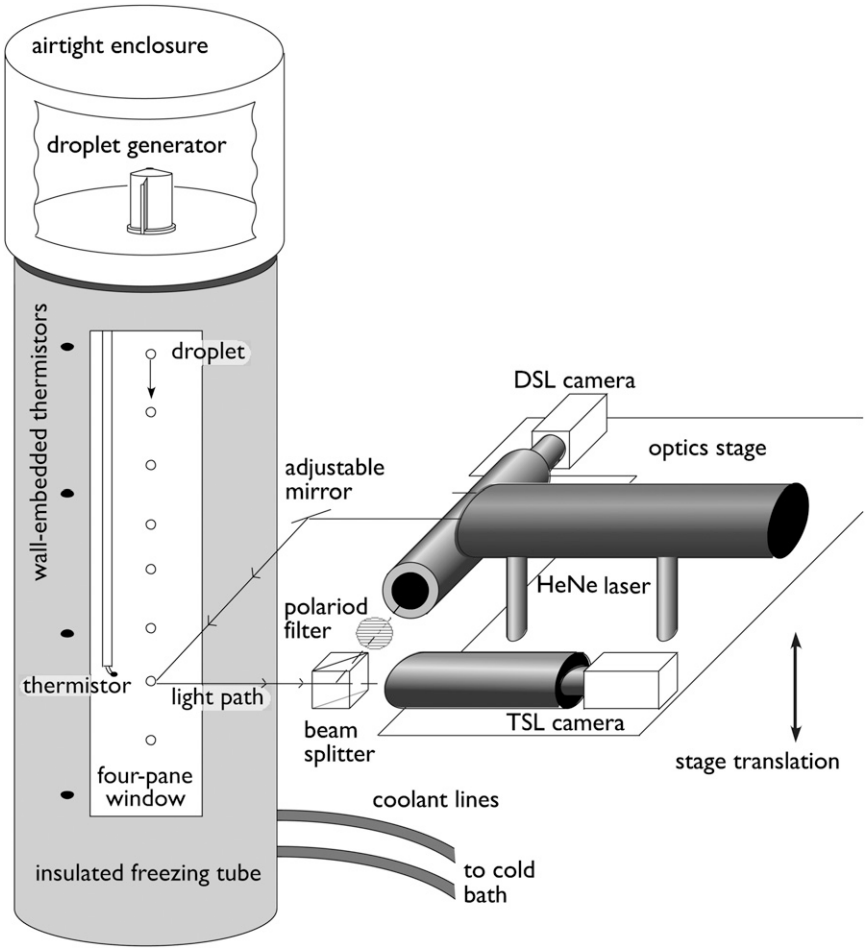

FIG. 1. Schematic drawing of droplet free-fall freezing tube apparatus.

maintained at near room temperature while the bottom of the freezing tube was maintained at about −85°C. The freezing tube is surrounded by thermal insulation and has a pair of opposing four-pane windows oriented vertically along the tube sides for illumination and to allow imaging of the droplet stream. A small circular window just below the droplet generator provides for imaging of the droplets just after emission from the generator. The droplet phase-detection system consists of two video cameras (one with and one without a polarizer) connected to tele-microscopic lenses that view the same region of the droplet stream through a beam splitter. The video cameras, beam splitter, and a polarized He-Ne laser are mounted on a translation stage that can be positioned at any height of interest along the freezing tube vertical axis.

In this paper, frozen-fraction curves $F(T)$ are measured at ambient pressure (1020 mb) for ammonium sulfate droplets with concentrations ranging from $0 < x < 33$ wt% and for sulfuric acid droplets with concentrations ranging from $0 < x < 10$ wt%; the high-concentration limit was set by the lowest temperature that our cryogenic bath unit could provide. Ammonium sulfate solutions were prepared by mixing high-purity liquid chromatography (HPLC) grade water with 40 wt% $(NH_4)_2SO_4$ (99.99% purity from Aldrich Chemical). Sulfuric acid solutions were prepared by mixing HPLC-grade water with H_2SO_4 (99.999% purity from Aldrich Chemical). Dilutions were typically mixed to better than 0.05 wt% accuracy.

The freezing tube and droplet generator enclosure were sealed from surrounding laboratory air and flushed with dry nitrogen gas for several hours during cool-down to avoid the potential injection of aerosol, thereby reducing the possibility of potential droplet–aerosol interaction effects to near zero. For each solution concentration of interest, droplets were emitted at about 5 Hz (to maximize emission rate while preventing droplet–droplet interactions during free-fall) from a single nozzle of a clean Hewlett-Packard inkjet cartridge

filled with about 4 ml of the solution. The initial droplet size was set by the droplet generator nozzle, and the droplets cooled as they fell down along the axis of the freezing tube. Droplet size changes during free-fall were of particular importance in these experiments because of the associated concentration changes. Ice reservoirs attached to the interior sides and bottom of the freezing tube were filled with water and frozen to maintain the relative humidity with respect to ice (RH_i) $\sim$ 100% along the droplet stream to reduce growth or evaporation of the droplets during free-fall.

The fraction of frozen droplets at a particular height (or temperature) was found by positioning the phase detection system at the height of interest and recording onto videotape about 2 min of both the total scattered light (TSL) and the depolarized scattered light (DSL) streak images. At a particular height it was usually quite evident when the majority of droplets were liquid or frozen by simply looking on the video screen to see whether streaks could be seen only in the TSL image (liquid) or in both the DSL and TSL images (solid). The frozen droplets were identified using the fact that light scattered from liquid droplets remains polarized in the laser's original plane of polarization, whereas some backscattered light from frozen droplets is depolarized because of droplet asphericity, cracks, bumps, surface roughness, and birefringence. The frozen-fraction curves were measured by translating the phase-detection system down to where 100% of the droplets are frozen and then making measurements at intervals between 100% and 0% of frozen-fraction. Each streak image was later analyzed by first subtracting the background intensity and then calculating the ratio DSL/TSL. Those particles with DSL/TSL above some threshold value (typically about 7% of full-scale intensity) were defined to be frozen and those below that threshold, liquid. The threshold value was set by comparing various datasets and requiring droplets to be all liquid at high temperatures and all solid at temperatures far below the nucleation temperature (essentially, at the lowest temperatures at the bottom of the freezing tube). Once the threshold was determined, frozen-fraction curves were obtained for a particular solution concentration by counting the number of droplets with DSL/TSL above and below the threshold value at each tube height (temperature). Results were insensitive to variations in threshold value so long as the criteria above were satisfied. Typically the DSL/TSL ratio was obtained from 200–400 droplets at each temperature, and the freezing of 3000–4000 droplets was analyzed for a single frozen-fraction curve.

In the results presented here, the droplet size was not monitored simultaneously with the streak images. Instead, after each frozen-fraction curve, a strobe light was used to make shadow images at 7× magnification (about 1 μm per pixel) at three or more heights along the droplet stream. A model (see Larson 2004) was used to calculate the droplet temperature at various heights in the freezing tube, correcting for temperature lag or lead due to droplet evaporation–growth or fall-speed effects. The inputs to the model were freezing tube temperatures (from a series of thermistors imbedded into the tube sides and from a thermistor attached to the bottom of a glass rod that can be slid up and down along the tube axis within a few mm of the droplet stream) and the droplet diameter at various heights obtained from the strobe images of the droplets [for more details, see Wood et al. (2002)].

3. Results

The solid symbols in Fig. 2 are examples of frozen-fraction curve data from this study for droplets containing pure water, 25 wt% $(NH_4)_2SO_4$, and 9.95 wt% H_2SO_4. The lines in Fig. 2 for each concentration are the best-fit parameterization:

$$F(T) = 1 - \frac{1}{1 + e^{-At}}, \tag{4}$$

with $t = T - T_f$. In this parameterization, the free parameters T_f and A are fit for each $F(T)$ and the freezing temperature T_f is the temperature where 50% of the droplets are frozen. The $F(T,x = 25$ wt% $(NH_4)_2SO_4)$ and $F(T,x = 9.95$ wt% $H_2SO_4)$ are quite similar in shape and the T_f for these two solutions are nearly the same, -53.73°C versus -54.49°C. The temperature range over which $F(T,x = 25$ wt% $(NH_4)_2SO_4)$ and $F(T,x = 9.95$ wt% $H_2SO_4)$ goes from 10% to 90% frozen-fraction is more than 2°C—considerably greater than the less than 1°C observed for pure water. For both $(NH_4)_2SO_4$–H_2O and H_2SO_4–H_2O solutions, the slope of the frozen-fraction curve at $t = 0$ decreases as x increases. This result is consistent with the predictions of the TMPC. Because $F(T)$ is measured directly (usually with a precision of $\pm$1°C or better), the nucleation rate $J(T)$ (with units of m^{-3} s^{-1}) can be calculated by inverting

$$F(T) = 1 - \exp\left[\frac{-V_d}{\dot{T}}\int_0^T J(T')dT'\right], \tag{5}$$

where V_d is the droplet volume, $\dot{T} = dT/dz \times v_{\text{term}}$ is the cooling rate, $dT/dz = 1.5°$–$1.9°$C cm^{-1} is the temperature gradient experienced by a droplet when falling down the freezing tube, and v_{term} is the droplet terminal velocity. The trend of $J(T)$ versus solution concentration is illustrated in Fig. 7 of Larson and Swanson

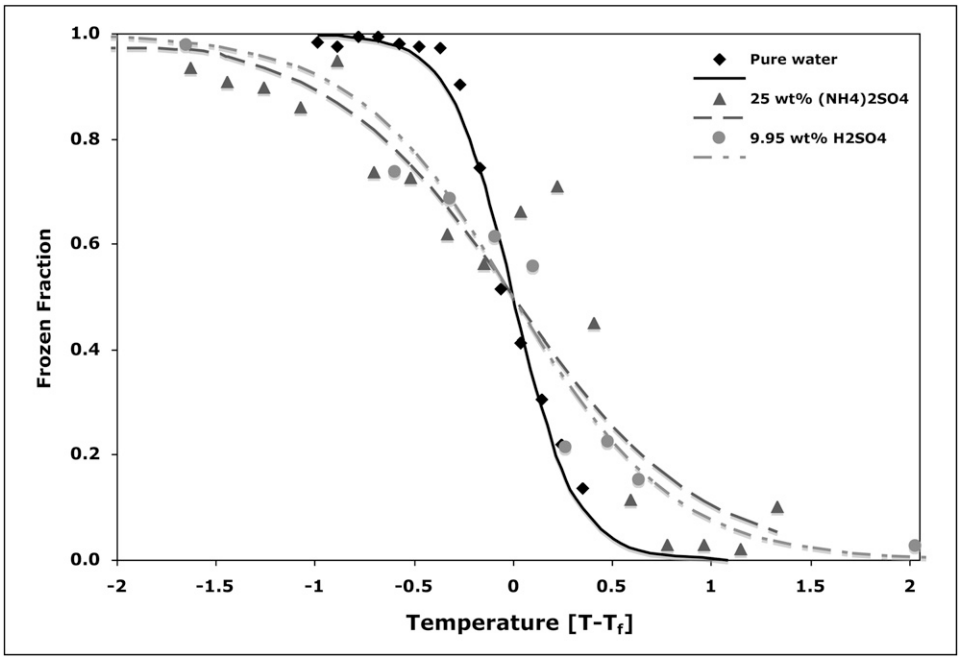

FIG. 2. Frozen-fraction curve for pure water, 25 wt% $(NH_4)_2SO_4$–H_2O, and 9.95 wt% H_2SO_4–H_2O solutions. Lines are the best fit to the Eq. (1) parameterization for each $F(T)$.

(2006). Note that $d\log(J)/dT|_{t=0}$ for 25 wt% $(NH_4)_2SO_4$ and 9.95 wt% H_2SO_4 is considerably larger (about $-0.4°C^{-1}$) than for pure water (about $-1°C^{-1}$).[3] For these two solutes, $d\log(J)/dT|_{t=0}$ correlates much better with T_f than with either a_w or x.

The solid red circles in Fig. 3 are my T_f results for $(NH_4)_2SO_4$–H_2O solution droplets with diameters ranging from 30 to 50 μm. The solid red circles in Fig. 4 are my T_f results for H_2SO_4–H_2O solution droplets with diameters ranging from 56 to 70 μm. All data points plotted in Figs. 3 and 4 are shown in terms of water activity using the Clegg aqueous solution model (Clegg et al. 1998) to convert aqueous $(NH_4)_2SO_4$ or H_2SO_4 concentrations to water activity. Each of the data points in this study represents the average T_f from multiple measurements of $F(T)$. In general, for both solutions the droplet diameter remained nearly constant—less than 2 μm change (tube top versus tube bottom) for the $(NH_4)_2SO4$–H_2O dataset and less than 3 μm change for the H_2SO_4–H_2O dataset—and no consistent growth or evaporation of the droplets was observed during free-fall.

4. Discussion

The open blue symbols in Figs. 3 and 4 are the T_f results from all datasets published over the past decade for the freezing of $(NH_4)_2SO_4$–H_2O and H_2SO_4–H_2O solution aerosols or droplets that also reported an associated solution concentration.[4] In plotting these datasets together, the implied assumption is that the aerosol composition is known and well constrained (as each publication claims) and that each measured T_f is the homogeneous freezing temperature for aerosol or liquid droplets with the specified solute composition. [Conversion from solution concentration to a_w has been made using the Clegg aqueous solution model (Clegg et al. 1998).] This method of comparison (with the same assumption) is used to establish the water activity idea and the TMPC theory in Fig. 1b of Koop et al. (2000). In the appendix, I discuss whether homogeneous freezing under identical conditions is occurring in these experiments or whether, in many cases, heterogeneous processes may be intervening. The black dashed line in Figs. 3 and 4, calculated using Eq. (3), is the melting point curve; the center line of the gray shaded region marked $\Delta a_w = 0.305$ [see Eq. (2)] is the TMPC with $\Delta a_w = 0.305$. The TMPC with $\Delta a_w = 0.305$ is consistent with the T_f data from 18 different aqueous solutions (see Fig. 1b in Koop et al. 2000) but the agreement is not

[3] These pure water findings are in rough agreement with DeMott and Rogers (1990).

[4] Data for solution concentrations larger than the eutectic concentration (which for aqueous ammonium sulfate is 40 wt% and for aqueous sulfuric acid is 35.3 wt%) are not shown here because the TMPC theory does not predict solute independence for concentrations around the a_w of the various eutectics.

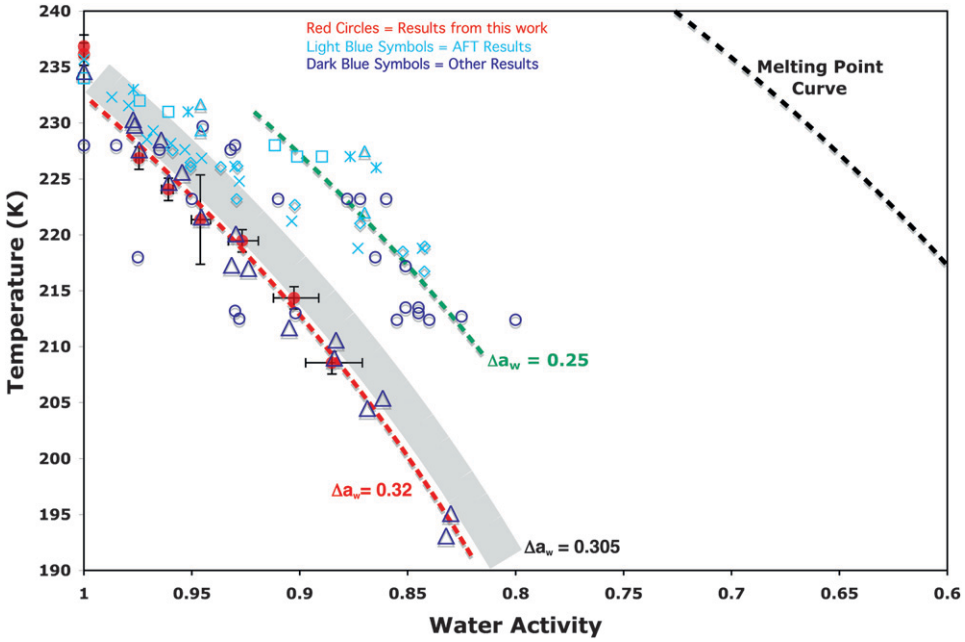

FIG. 3. Results for $(NH_4)_2SO_4$–H_2O solution freezing. Data from this study (solid red circles) with $a_w < 0.98$ are shown with a best-fit TMPC (dashed red line) with $\Delta a_w = 0.32$. The T_f from other recent experiments are shown with open blue symbols: Bertram et al. (2000; DSC and OM): large △; Chen et al. (2000; CFDC–wet): ○; Cziczo and Abbatt (1999; AFT): □; Prenni (2001b; AFT): × ; Chelf and Martin (2001; AFT): * ; Hung et al. (2002; AFT): ◇ ; Wise et al. (2004; AFT): small Δ. Also plotted are the melting-point curve (dashed black curve) and the TMPC with $\Delta a_w = 0.305$ (center line of gray curve). Vertical error bars of ±1°C are 1σ errors due primarily to the uncertainty in determining the actual droplet temperature. Horizontal error bars are dominated by the uncertainty in determining droplet diameter from strobe images of the droplets and assume a droplet concentration change associated with a droplet diameter change of $\pm 2\mu$m.

exact—the data form a cloud of points overlaying the TMPC with a scatter or spread in a_w of about ±0.015 (indicated in both Figs. 3 and 4 by the width of the gray shaded region centered on the TMPC).

The complete dataset plotted in Fig. 3 for $(NH_4)_2SO_4$–H_2O solutions [only the Bertram et al. (2000) result was used in the Koop et al. (2000) TMPC analysis] was obtained using a number of techniques: aerosol flow tube (AFT) with infrared spectroscopy detection (Cziczo and Abbatt 1999; Chelf and Martin 2001; Prenni et al. 2001b; Hung et al. 2002; Wise et al. 2004), optical microscope (OM) and differential scanning calorimetry (DSC) (Bertram et al. 2000), and continuous flow thermal diffusion chamber (CFDC) [data points marked "wet" from Chen et al. (2000)]. The freezing tube $(NH_4)_2SO_4$–H_2O dataset (see Fig. 3) is consistent with the OM and DSC studies (Bertram et al. 2000) and the low-temperature CFDC datum (Chen et al. 2000); these are the lowest-temperature T_f results for ammonium sulfate solutions. Once corrections are made for transient cooling rate effects, the lowest-temperature T_f results are most likely the result of homogeneous nucleation because I suggest that the homogeneous freezing temperature is the lowest temperature that a liquid solution can have. The red dotted line in Fig. 3 is the TMPC with $\Delta a_w = 0.320$, a curve that agrees well with the Bertram et al. (2000) results and the freezing tube dataset for $0.8 < a_w < 0.98$ but does not pass through (within the 1σ errors) the pure water freezing data point at $a_w = 1$. This dotted red line appears to be a relatively good lower bound for the lowest T_f results for the freezing of $(NH_4)_2SO_4$ solutions with $0.98 > a_w > 0.8$. Both the Bertram et al. (2000) results and the freezing tube $(NH_4)_2SO_4$–H_2O dataset fall somewhat below the gray shaded region surrounding the TMPC with $\Delta a_w = 0.305$, although some of the freezing tube 1σ error bars fall within the shaded region. To the 1σ level, the freezing tube dataset is inconsistent with the TMPC with $\Delta a_w = 0.305$ [even taking into account that the TMPC curve corresponds to $J(T) = 10^{10}$ cm^{-3} s^{-1} compared with $J(T) = 10^8$ cm^{-3} s^{-1} for the freezing tube dataset]. A curve shaped like the TMPC but with $\Delta a_w = 0.32$ does appear to approximate both the freezing tube dataset and the other lowest-temperature T_f datasets, with $0.98 > a_w > 0.8$, for ammonium sulfate.

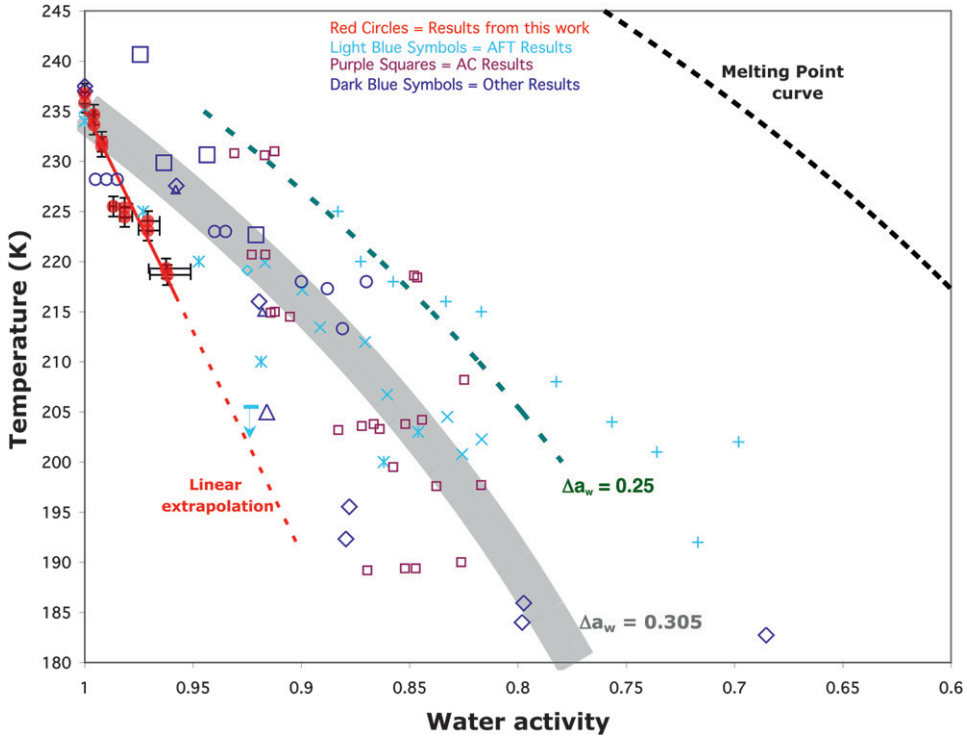

FIG. 4. Results for H_2SO_4–H_2O solution freezing. Data from this study (solid red circles) are plotted with a best-fit line (solid red line) and a linear extrapolation to lower temperatures (dashed red line). The T_f from other recent experiments are shown with open blue symbols: Bertram et al. (1996; AFT): +; Krämer (1998; EDB): small Δ; Koop et al. (1998; OM): blue-gray dotted line within the gray curve; Chen et al. (2000; CFDC): ○; Vortisch et al. (2000; EDB): large ◇; Cziczo and Abbatt (2001; AFT): *; Chelf and Martin (2001; AFT): –; Prenni (2001b; AFT): ×; Möhler et al. (2003; AC): small □; Ettner et al. (2004; AL): large □; Bogdan et al. (2006; DSC): large Δ; Beaver et al. (2006; AFT): small ◇. The arrow below the (–) datum indicates freezing was not observed above this temperature. Also plotted are the melting-point curve (dashed black curve) and the TMPC with $\Delta a_w = 0.305$ (center line of gray curve). Vertical error bars of ±1°C are 1σ errors due primarily to the uncertainty in determining the actual droplet temperature. Horizontal error bars are dominated by the uncertainty in determining droplet diameter from strobe images of the droplets and assume a droplet concentration change associated with a droplet diameter change of ±3μm.

The complete dataset plotted in Fig. 4 for H_2SO_4–H_2O solutions [only the Koop et al. (1998) result was used in the Koop et al. (2000) TMPC analysis] was obtained using an AFT (Bertram et al. 1996; Cziczo and Abbatt 2001; Prenni et al. 2001b; Chelf and Martin 2001; Beaver et al. 2006), OM (Koop et al. 1998), electrodynamic balance (EDB) (Krämer 1998; Vortisch et al. 2000), CFDC (Chen et al. 2000), aerosol chamber (AC) (Möhler et al. 2003), acoustic levitator (AL)) (Ettner et al. 2004), and DSC (Bogdan et al. 2006). The freezing tube dataset for H_2SO_4–H_2O solutions (see Fig. 4) is consistent with the lowest-temperature AFT and CFDC data and is described well by a best-fit linear parameterization [$T_f(a_w) = 441.59a_w - 206.47$, shown as the solid red line in Fig. 4]. Figure 4 also shows some nonlinearities (some being as large as the 1-σ errors) in the freezing tube dataset that I cannot explain at present. The slope of the TMPC in the region of $a_w > 0.96$ is much less steep than both the freezing tube data and the other lowest T_f results. Clearly the TMPC with $\Delta a_w \sim 0.32$ does not pass through each sulfuric acid freezing tube data point within the 1-σ error bars and a single $T_f(a_w)$ curve does not describe our T_f results for both ammonium sulfate and sulfuric acid aqueous solutions.

Figures 3 and 4 illustrate what appears to be a large amount of disparity between the laboratory datasets (a fact noted by a number of experimenters; see Chen et al. 2000; Cziczo and Abbatt 1999, 2001; Chelf and Martin 2001; Prenni et al. 2001b; Hung and Martin 2001; DeMott 2002; Hung et al. 2002; Wise et al. 2004; Larson and Swanson 2006; Abbatt et al. 2006), and most of these T_f datasets fall outside the $a_{w-f}(T) \pm 0.015$ shaded region surrounding the TMPC that characterizes the cloud of data points from 18 different aqueous

solutions (Koop et al. 2000). It is beyond the scope of this paper to construct the necessary detailed computational fluid dynamics model for each experimental apparatus (even if sufficient information were available). I suggest that the cause of the disparity between and scatter within the datasets is a variety of heterogeneous processes[5] that intervene before homogeneous nucleation occurs and in addition disrupt our knowledge of the solute concentration. See the appendix for a more detailed discussion of this issue.

5. Atmospheric implications

In this section, the implications of an extrapolation of my aqueous sulfuric acid $T_f(a_w)$ results are explored in relation to recent observations of persistent and unexpectedly high ice supersaturations in some regions of the upper troposphere. The TMPC theory predicts that $RH_i \sim 1.6$ is required for ice to form on or in existing aerosol particles (Koop et al. 2000; Koop 2004). But RH_i values above 2.0 have been observed when crossing the tropical tropopause in cloud-free regions (Jensen et al. 2005) and peak RH_i values approaching water saturation levels are sometimes observed in ice particle–free regions (Heymsfield et al. 1998; Jensen et al. 2001). These values are much higher than predicted by current cloud models and are too high if liquid aerosol particles had frozen at the temperature predicted by the TMPC (Peter et al. 2006). Also, microwave limb sounding data (Spichtinger et al. 2002; Gettleman et al. 2006; Treffeisen et al. 2007) show no sharp cutoff above $RH_i = 1.6$, which might be expected if the TMPC set an upper bound for tropospheric RH_i.

Why is the humidity in the upper troposphere sometimes found to be so high? Some suggest that transient non-steady-state conditions and instrumental calibration errors in airborne water vapor measuring equipment may be larger than expected, but to date no experimental evidence for these possibilities has been published. If these measurements reflect the actual water vapor present in these regions, then several possible causes have been proposed in an attempt to understand these puzzling results: 1) chemical impurities might perturb the equilibrium relative humidity (Tabazadeh et al. 1998; Gao et al. 2004); 2) the equilibrium vapor pressure extrapolations to temperatures below −40°C may be erroneous [these models are constructions that have not been well checked against actual laboratory measurements (Clegg et al. 1998; Murphy and Koop 2005)]; 3) metastable cubic ice—with a higher equilibrium vapor pressure than hexagonal ice—may be present (Murray et al. 2005; Shilling et al. 2006b); 4) residual water vapor from evaporating ice particles may be present (Keith 2000); or 5) high-velocity updrafts and rapid dynamics may introduce considerable humidity into these regions (Gayet et al. 2006). Alternatively, Peter et al. (2006) suggests that our current understanding of the principles underlying ice cloud formation and evolution may not be correct.

I propose another possibility: sulfuric acid aerosol, a species often found in upper-tropospheric regions, may freeze at temperatures considerably lower than predicted by the TMPC. This suggestion is based on the speculative linear extrapolation of my sulfuric acid freezing tube dataset. The linear extension of the best-fit linear parameterization (dotted red line in Fig. 4) is consistent with the lowest-temperature DSC, EDB, AC, and AFT data points (no freezing at temperatures above 205.5 K), and a quadratic extrapolation does not significantly improve the fit over the linear extrapolation. One expects increased supercooling with increasing solute concentration, and an extrapolation with curvature like that of the TMPC would show an even larger deviation from the TMPC with $a_w \sim 0.32$, but then the $S^*_{ice} \sim 2$ contour in Fig. 5 would be for a larger droplet size. More experimental data from methodologies that can continuously follow solute concentration are needed to check this extrapolation experimentally for T_f below 215 K, but the dotted red line in Fig. 4 is a relatively good lower bound for the lowest T_f results for H_2SO_4–H_2O solutions with $a_w > 0.8$.

I use this relation to calculate the critical ice saturation ratio defined as

$$S^*_{ice} = P^*_{water\text{-}sol}(T_f)/P_{ice}(T_f), \quad (6)$$

where $P^*_{water\text{-}sol}(T_f)$ is the equilibrium water partial pressure of the liquid solution at freezing point temperature T_f and $P_{ice}(T_f)$ is the vapor pressure of ice (also at T_f). My predictions for S^*_{ice} for 30-μm, 20-nm, and 10-nm aerosol particles (assuming no vertical velocity but including the Kelvin effect, which increases vapor pressure due to a droplet's curvature) are shown with thick purple lines in Fig. 5. Figure 5 also shows the results from in situ measurements of ice saturation ratio, temperature, and water vapor concentration made by Jensen et al. (2005) during a WB-57 aircraft descent across the tropopause south of Costa Rica collected during a series of flights on 29 January 2004. During the descent water vapor concentration increased monotonically and temperature decreased with decreasing

[5] As opposed to a completely homogeneous (single phase) process, a heterogeneous process involves two or more phases (i.e., liquid–vapor, liquid–solid, liquid–vapor–substrate, etc).

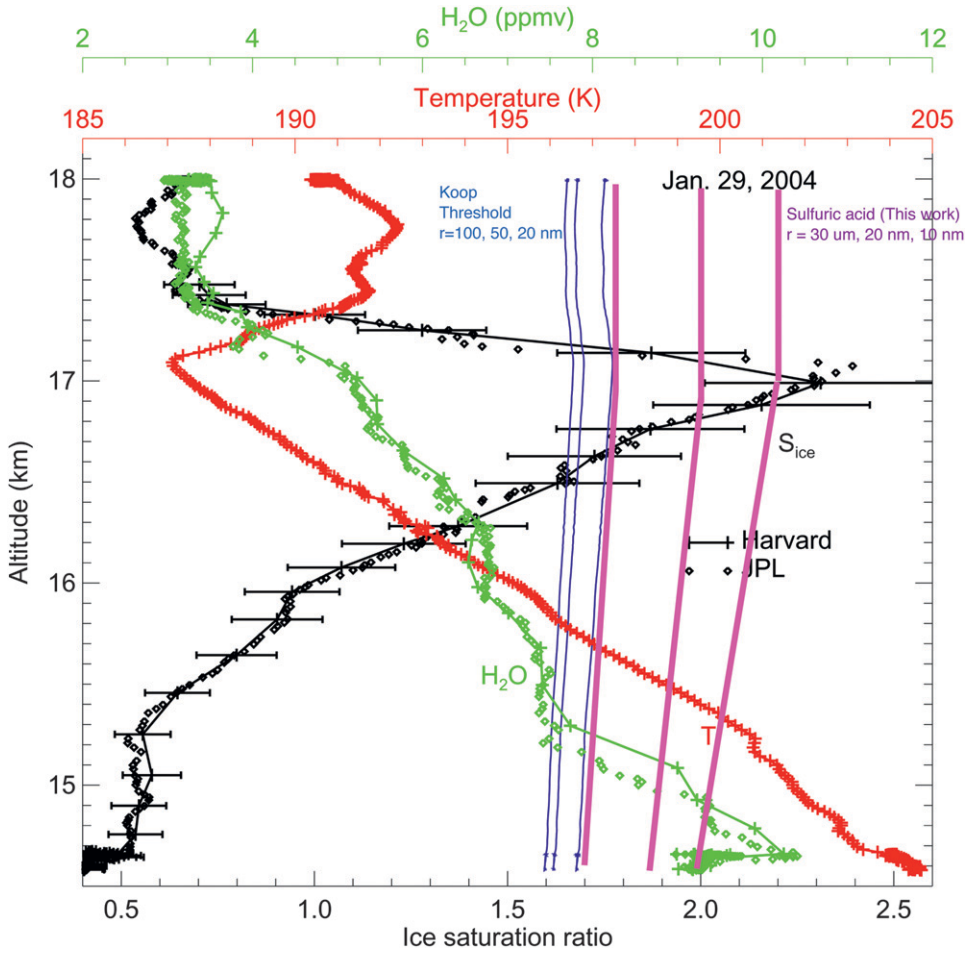

FIG. 5. Ice supersaturation ratio, temperature, and water vapor concentration measurements during a transit across the tropical tropopause south of Costa Rica (see color coding; plot is after Jensen et al. 2005). The thin blue lines are the saturation ratio predictions from the TMPC for 100-, 50-, and 20-nm aerosol particles and the thick purple lines are the saturation ratio prediction for 30-μm, 20-nm, and 10-nm aerosol particles from a linear extrapolation of our H_2SO_4-H_2O freezing data. The observed ice saturation ratio is much larger than the predictions of the TMPC but is consistent with the predictions for 20- and 10-nm aerosol particles using our T_f data.

altitude down to the tropopause (187 K) at 17.1 km (which was observed to have a 5.2 ppmv water vapor concentration). These water vapor and temperature measurements correspond to an ice saturation ratio of 2.3–2.4 (or 130%–140% supersaturation with respect to ice), with an uncertainty in the saturation ratio of about 13%. Video ice particle sampler (VIPS) instrument images were also collected during the descent and indicate that no ice crystals larger than the detectible size of 10 μm were present within the supersaturated layer. The thin blue lines in Fig. 5 are the ice saturation ratio thresholds predicted by the TMPC with $\Delta a_w = 0.305$ for aerosol radii of 100, 50, and 20 nm. Even for small aerosol particles ($r \sim 20$ nm), the TMPC predicts these aerosol particles would have frozen at ice saturation ratios well below those measured in these field experiments; therefore, the subsequent depositional growth should have reduced the water vapor concentration considerably. This high RH_i is not explained by the TMPC theory, but our extrapolated T_f results for H_2SO_4–H_2O solution freezing for droplets 20 nm and smaller are consistent within the error bars with the highest observed ice saturation ratio measurements.

In the case of the Jensen et al. (2005) measurements, there is no direct confirmation that sulfuric acid aerosol droplets were present in this region. But simultaneous particle analysis by laser mass spectrometry (PALMS) measurements made on either side of the tropopause during their descent show the aerosol composition to be primarily mixed sulfates with organics; given the

expected mixing, these measurements indicate that the highly supersaturated air probably had these same components. Also, Nucleation-Mode Aerosol Size Spectrometer and Focused Cavity Aerosol Spectrometer data indicate the presence of aerosol concentrations consistent with lognormal aerosol size distributions (100 cm^{-3} with a mode radius of 25 nm), so it is perhaps likely that sulfuric acid aerosols were present.

Aerosol droplets that freeze heterogeneously at higher temperatures and lower supersaturations can alter cloud radiative properties by modifying the particle size distribution and number density and thus influence both the concentration of neighboring liquid droplets and the local RH_i (DeMott et al. 1997; Jensen and Toon 1997; Kärcher and Lohmann 2003; Abbatt et al. 2006). The freezing tube homogeneous freezing datasets for both aqueous ammonium sulfate and aqueous sulfuric acid solutions are consistent with the previous lowest T_f measured by a number of different techniques. If the linear extrapolation of the freezing tube dataset is accurate, then it seems that sulfuric acid aerosol droplets that freeze homogeneously at the lowest freezing-point temperatures can cause extremely high RH_i to persist in cloud-free regions of the upper troposphere.

6. Conclusions

From the freezing tube results I conclude that the water activity theory with a single $T_f(a_w)$ curve does not provide a good representation of the experimental data for the homogeneous freezing of both sulfuric acid and ammonium sulfate solutions. This calls into question the proposition that T_f for all solutions can be expressed as a thermodynamic property that depends on activity alone and that T_f can be viewed simply as a function of only a_w. Instead, it appears that water activity may provide a good indicator of T_f for some (Koop et al. 2000) but not all aqueous solutes. These results suggest that a single $T_f(a_w)$ characterization should not be used in cloud models as $T_f(S^*_{ice})$, where a_w and the supersaturation over ice S^*_{ice} are related for a given drop size via the Kelvin effect.

The work presented here suggests instead that two separate curves are required to represent the homogeneous $T_f(a_w)$ for these solutes. The datasets presented here also suggest that both Eq. (1) (the freezing temperature depression parameterization) with a single $\lambda \sim 1.7$ and Eq. (2) (the TMPC theory) with a single $\Delta a_w \sim 0.305$ do not provide a universal solute-independent relationship between the freezing and melting curves for all aqueous solutes and therefore do not provide a solute-independent prediction for the homogeneous T_f for all solutes. These conclusions are the result of evaluating both the freezing tube data and all recent T_f datasets. My findings are different from those of Abbatt et al. (2006), who considered only a subset of these T_f results. I suggest that homogeneous freezing is not the only process involved in some previous $(NH_4)_2SO_4$–H_2O and H_2SO_4–H_2O T_f measurements and that in some cases heterogeneous processes intervened, causing freezing temperatures and solute concentrations to appear scattered and trend too high.

Acknowledgments. I thank Ben Wearn for assistance with the sulfuric acid solution measurements and Ben Larson for assistance with the ammonium sulfate solution measurements. I thank Marcia Baker, Thomas Koop, Jon Nelson, Mary Laucks, and an anonymous reviewer for valuable comments on the manuscript. This work is supported by the National Science Foundation Grant ATM-0323930 and grants from the University of Washington Royalty Research Fund and the University of Washington Program for Climate Change.

APPENDIX

On the Disparity between and Scatter in Previous Datasets

The freezing tube methodology was designed to reduce to near zero the influence of potential competing heterogeneous processes and thereby observe only homogeneous freezing. This methodology has the advantage that droplet size (and therefore composition) can be continuously monitored throughout the freezing tube. Droplets are well separated and the tube is relatively aerosol-free because of the initial flushing of the tube. In addition, the droplet stream remains well away from the tube sides, so droplet–vapor wall effects and moistening–drying convective regions are minimal.

Classical nucleation theory predicts (given the experimental variation in droplet size and nucleation rate) that the datasets shown in Figs. 3 and 4 should lie in a band narrower than the width of the shaded region surrounding the TMPC. Experimentally, the scatter of the data points from 13 of the 19 datasets [as evidenced by the width of a constant-width region centered on the T_f of pure water ($a_w = 1$) and sufficiently wide to encompass all data points from each individual dataset] is approximately the width of the shaded region surrounding the TMPC or less. For only three of the 19 datasets are the data points scattered over a region more than 3 times wider than the shaded region surrounding the TMPC. What are the possible causes for

the greater than expected disparity among the 19 datasets?

The disparity–scatter is not likely due to contamination from soluble organic species because associated T_f shifts are found by recent experiments (Prenni et al. 2001a; DeMott et al. 2003; Wise et al. 2004; Zobrist et al. 2006) to be only a few °C or less—although the AL experiments (Ettner et al. 2004), using mm-size droplets and exhibiting some of the highest-temperature T_f, have had difficulty with contamination [originating perhaps from another species of contaminant (cf. Fig. 7 in Ettner et al. (2004)]. Also, the T_f datasets for aqueous sulfuric acid generally fall at a lower temperature than do those for ammonium sulfate, suggesting that ammonia or ammonium sulfate contamination is not likely significant in the sulfuric acid datasets. The large amount of scatter or spread in both the CFDC data in Fig. 3 and the AIDA AC data in Fig. 4 indicates that both datasets are consistent with most of the other results shown in their respective plots. The CFDC dataset includes data points for both a 0.1% and 1% activation threshold, but the temperature difference between these two thresholds is only a few °C and therefore this does not seem to be responsible for the majority of the scatter. The Mangold et al. (2005) AIDA AC result (not shown in Fig. 4 because they do not report an associated concentration) are consistent with the scatter of the Möhler et al. (2003) results and fall within and slightly above the gray-shaded region surrounding TMPC (Abbatt et al. 2006).

Based on ideas from many sources, I briefly discuss two possible hypotheses for the causes of the disparity/scatter. The first hypothesis, which has been explored in some detail by the Martin group (Chelf and Martin 2001; Hung and Martin 2001; Hung et al. 2002), is that homogeneous processes dominate within the various experiments and that systematic differences in aerosol size distributions, vapor-phase mass transfer, ice detection sensitivity, cooling rates, and residence times are responsible. Martin et al. conclude that for a subset of OM, DSC, CFDC, and AFT datasets no single $J(T)$ can be found that is consistent with these results. A calculation of $d\log(J)/dT$ [made using freezing tube $F(T)$ measurements like those shown in Fig. 2] gives results consistent with their findings and also suggests that differences in active fraction alone (which for the data shown in Figs. 3 and 4 may range from as low as 10^{-6} to 0.5) is not likely the sole cause of the disparity-scatter. Despite this analysis and the paucity of direct experimental evidence, this hypothesis remains viable but, in my view, unlikely to explain completely the disparity-scatter.

An alternative hypothesis is that in many of the previous experiments, heterogeneous processes (processes occurring at the interface between two phases or associated with a substrate) dominate and intervene before homogeneous nucleation can occur and so cause droplet solute concentrations to be less well known and controlled than the published reports suggest—particularly in those experiments that cannot continuously monitor aerosol composition in all regions of the apparatus. Here are a few examples of potentially important heterogeneous processes. Convection, induced by apparatus geometry and temperature gradients, appears from computational fluid dynamics studies to be more intense than previously assumed, perhaps leading to enhanced and more sustained aerosol–vapor wall interactions and moistening–drying episodes and longer residence times (Khalizov et al. 2006b). A mixed homogeneous–heterogeneous process whereby immersion- or deposition-mode nucleation occurs under certain conditions in liquid ammonium sulfate droplets has been observed (Zuberi et al. 2001; Zobrist et al. 2006; Shilling et al. 2006a; Abbatt et al. 2006). [Although sulfuric acid cannot crystallize under ordinary laboratory conditions, larger temperature gradients in these experiments may enhance moistening-drying events (Khalizov et al. 2006b) and, in addition, cause aerosol surface processes to become increasingly important (Tabazadeh et al. 2002b; Kay et al. 2003; Tabazadeh et al. 2002a).] Mixed-phase and undetected early nucleation in upstream aerosol have been suggested as problems in some AFT experiments (Hung and Martin 2002; Hung et al. 2002; Chelf and Martin 2001; Hung and Martin 2001; Cziczo and Abbatt 1999), although these processes have yet to be modeled in detail or have their influence quantified experimentally. The IR spectroscopy methodology used in the AFT experiments needs a determination of the detection limit for solid aerosol particles because there may be more solid aerosol upstream than has been previously suggested by simply monitoring the peak shape of the NH_4^+ peaks (such a calibration would settle questions regarding potential ice particle undercounting or overcounting, particularly in the presence of haze particles). Frost was reported present on many of the AFT experiment tube walls and the potential process of splintering and enhanced vapor-phase mass transfer may be quite important (Khalizov et al. 2006b); this issue requires further evaluation. The AFT results taken together (light blue symbols in both Figs. 3 and 4) show some of the largest disparity despite the fact that the individual AFT datasets are remarkably precise, suggesting that a heterogeneous process (characterized by the $\Delta a_w = 0.25$ curve shown in both Figs. 3 and 4) is apparently also active in some experiments. For both ammonium sulfate and sulfuric acid solutions, the droplets used in the freezing tube experiments were

much larger and froze at lower temperatures than the aerosol particles used in the AFT experiments—which is opposite to the behavior expected on the basis of size difference (Pruppacher and Klett 1997). Questions regarding the assumptions used in the analysis of the AFT results warrant a closer look; although the disparity in previous AFT results provides a caution to future AFT experimenters, improved AFT methods are being developed that may reduce the influence of many potential problematic processes (Khalizov et al. 2006a).

For ammonium sulfate the DSC and OM results (Bertram et al. 2000) are self-consistent and consistent with the freezing tube results; however, the sulfuric acid results are not consistent and the OM results occur at warmer T_f. I suspect the OM ammonium sulfate results are consistent with the freezing tube results because the OM methodology has the advantage that droplets are placed on a hydrophobic glass substrate, which can be continuously monitored during the freezing process to assess potential droplet size and associated solute concentration variations, and because both the substrate-based OM technique and the oil emulsion–based DSC technique give similar results—providing evidence that the substrate was sufficiently well passivated by the organosilane coating and the oil–solution interface remained passive. For the sulfuric acid datasets both the freezing tube and OM droplet size and $J(T)$ were very similar and the small differences do not account for the difference in the measured T_f. The disadvantage of substrate- and interface-based methodologies is that the passivation will eventually fail at lower temperatures and for more corrosive solutes. For sulfuric acid the associated DSC measurements were not done, and although the OM dataset (Koop et al. 1998) is extremely smooth (and falls fully within the shaded region surrounding the TMPC), one has no indication of the state of the substrate passivation. It has been shown that the heterogeneous freezing process can be well regulated by interactions at the solution–substrate interface (e.g., see Seeley and Seidler 2001) and smooth curves are the result. I suspect therefore that a substrate-induced heterogeneous process is acting in the OM sulfuric acid experiments.

A final consideration is that a_w is calculated using aqueous solution models like that of Clegg et al. (1998), and although the accuracy of the aqueous solution model does not affect the disparity between or scatter in the data (because the same model was used for all data), the degree to which datasets for different solutes are consistent with the TMPC may to some extent be an artifact of the aqueous solution model. Aqueous solution models require validation by experimental data, but few measurements have been made of low-temperature vapor pressures over supercooled solutions. Therefore, to some unknown extent, the conversion of x to a_w is uncertain (Clegg et al. 1998, 1995) and there has been some discussion regarding the accuracy of these models at low temperatures (Knopf et al. 2003; Clegg and Brimblecombe 2005; Knopf et al. 2005).

REFERENCES

Abbatt, J. P. D., S. Benz, D. J. Cziczo, Z. Kanji, U. Lohmann, and O. Möhler, 2006: Solid ammonium sulfate aerosols as ice nuclei: A pathway for cirrus cloud formation. *Science,* **313,** 1770–1773.

Baker, M. B., 1997: Cloud microphysics and climate. *Science,* **276,** 1072–1078.

——, and M. Baker, 2004: A new look at homogeneous freezing of water. *Geophys. Res. Lett.,* **31,** L19102, doi:10.1029/2004GL020483.

Beaver, M. R., M. J. Elrod, R. M. Garland, and M. A. Tolbert, 2006: Ice nucleation in sulfuric acid/organic aerosols: Implications for cirrus cloud formation. *Atmos. Chem. Phys.,* **6,** 3231–3242.

Bertram, A. K., D. D. Patterson, and J. J. Sloan, 1996: Mechanisms and temperatures for the freezing of sulfuric acid aerosols measured by FTIR extinction spectroscopy. *J. Phys. Chem.,* **100,** 2376–2383.

——, T. Koop, L. T. Molina, and M. J. Molina, 2000: Ice formation in $(NH_4)_2SO_4$-H_2O particles. *J. Phys. Chem.,* **104A,** 584–588.

Bogdan, A., M. J. Molina, K. Sassen, and M. Kulmala, 2006: Formation of low-temperature cirrus from H_2SO_4/H_2O aerosol droplets. *J. Phys. Chem. Lett.,* **110,** 12 541–12 542.

Chelf, J. H., and S. T. Martin, 2001: Homogeneous ice nucleation in aqueous ammonium sulfate aerosol particles. *J. Geophys. Res.,* **106,** 1215–1226.

Chen, Y., P. J. DeMott, S. M. Kreidenweis, D. C. Rogers, and D. E. Sherman, 2000: Ice formation by sulfate and sulfuric acid aerosol particles under upper-tropospheric conditions. *J. Atmos. Sci.,* **57,** 3752–3766.

Clegg, S. L., and P. Brimblecombe, 2005: Comment on the ''Thermodynamic dissociation constant of the bisulfate ion from raman and ion interaction modeling studies of aqueous sulfuric acid at low temperatures.'' *J. Phys. Chem.,* **109A,** 2703–2706.

——, S. Ho, C. Chan, and P. Brimblecombe, 1995: Thermodynamic properties of aqueous $(NH_4)_2SO_4$ to high supersaturation as a function of temperature. *J. Chem. Eng. Data,* **40,** 1079–1090.

——, P. Brimblecombe, and A. S. Wexler, 1998: Thermodynamic model of the system $H^+ - NH_4^+ - SO_4^{2-} - NO_3^- - H_2O$ at tropospheric temperatures. *J. Phys. Chem.,* **102A,** 2137–2154. [Liquid solution model is available at http://www.aim.env.uea.ac.uk/aim/aim.htm.]

Cziczo, D. J., and J. P. D. Abbatt, 1999: Deliquescence, efflorescence, and supercooling of ammonium sulfate aerosols at low temperature: Implications for cirrus cloud formation and aerosol phase in the atmosphere. *J. Geophys. Res.,* **104,** 13 781–13 790.

——, and ——, 2001: Ice nucleation in NH_4HSO_4, NH_4NO_3, and H_2SO_4 aqueous particles: Implications for cirrus cloud formation. *Geophys. Res. Lett.,* **28,** 963–966.

DeMott, P. J., 2002: Laboratory studies of cirrus cloud processes. *Cirrus,* D. K. Lynch et al., Eds., Oxford University Press, 102–135.

——, and D. C. Rogers, 1990: Freezing nucleation rates of dilute solution droplets measured between −30° and −40°C in laboratory simulations of natural clouds. *J. Atmos. Sci.,* **47,** 1056–1064.

——, M. P. Meyers, and W. R. Cotton, 1994: Parameterization and impact of ice initiation processes relevant to numerical model simulations of cirrus clouds. *J. Atmos. Sci.,* **51,** 77–90.

——, D. C. Rogers, and S. M. Kreidenweis, 1997: The susceptibility of ice formation in upper tropospheric clouds to insoluble aerosol components. *J. Geophys. Res.,* **102,** 19 575–19 584.

——, D. J. Cziczo, A. J. Prenni, D. M. Murphy, S. M. Kreidenweis, D. S. Thompson, R. Borys, and D. C. Rogers, 2003: Measurements of the concentration and composition of nuclei for cirrus formation. *Proc. Natl. Acad. Sci. USA,* **100,** 14 655–14 660.

Ettner, M., S. K. Mitra, and S. Borrmann, 2004: Heterogeneous freezing of single sulfuric acid solution droplets: Laboratory experiments utilizing an acoustic levitator. *Atmos. Chem. Phys.,* **4,** 1925–1932.

Gao, R. S., and Coauthors, 2004: Evidence that nitric acid increases relative humidity in low-temperature cirrus clouds. *Science,* **303,** 516–520.

Gayet, J., and Coauthors, 2006: Microphysical and optical properties of midlatitude cirrus clouds observed in the Southern Hemisphere during INCA. *Quart. J. Roy. Meteor. Soc.,* **132,** 2719–2748.

Gettleman, A., E. J. Fetzer, A. Eldering, and F. W. Irion, 2006: The global distribution of supersaturation in the upper troposphere from the atmospheric infrared sounder. *J. Climate,* **19,** 6089–6103.

Haag, W., B. Kärcher, J. Strom, A. Minikin, U. Lohmann, J. Ovarlez, and A. Stohl, 2003: Freezing thresholds and cirrus cloud formation mechanisms inferred from in-situ measurements of relative humidity. *Atmos. Chem. Phys.,* **3,** 1791–1806.

Heymsfield, A. J., and R. M. Sabin, 1989: Cirrus crystal nucleation by homogeneous freezing of solution droplets. *J. Atmos. Sci.,* **46,** 2252–2264.

——, and L. M. Miloshevich, 1993: Homogeneous ice nucleation and supercooled liquid water in orographic wave clouds. *J. Atmos. Sci.,* **50,** 2335–2353.

——, ——, C. Twohy, G. Sachse, and S. Oltmans, 1998: Upper-tropospheric relative humidity observations and implications for cirrus ice nucleation. *Geophys. Res. Lett.,* **25,** 1343–1346.

Hung, H.-M., and S. T. Martin, 2001: Apparent freezing temperatures modeled for several experimental apparatus. *J. Geophys. Res.,* **106,** 20 379–20 394.

——, and ——, 2002: Infrared spectroscopic evidence for the ice formation mechanisms active in aerosol flow tubes. *Appl. Spectrosc.,* **56,** 1067–1081.

——, A. Malinowski, and S. T. Martin, 2002: Ice nucleation kinetics of aerosols containing aqueous and solid ammonium sulfate particles. *J. Phys. Chem.,* **106A,** 293–306.

Jeffery, C. A., and P. H. Austin, 1997: Homogeneous nucleation of supercooled water: Results from a new equation of state. *J. Geophys. Res.,* **102,** 25 269–25 279.

Jensen, E. J., and O. B. Toon, 1997: The potential impact of soot particles from aircraft exhaust on cirrus clouds. *Geophys. Res. Lett.,* **24,** 249–252.

——, ——, D. L. Westphal, S. Kinne, and A. J. Heymsfield, 1994: Microphysical modeling of cirrus. 1. Comparison with 1986 FIRE IFO measurements. *J. Geophys. Res.,* **99,** 10 421–10 442.

——, and Coauthors, 1998: Ice nucleation processes in upper tropospheric wave-clouds observed during SUCCESS. *Geophys. Res. Lett.,* **25,** 1363–1366.

——, L. Pfister, A. S. Ackerman, A. Tabazadeh, and O. B. Toon, 2001: A conceptual model of the dehydration of air due to freeze-drying by optically thin, laminar cirrus rising slowly across the tropical tropopause. *J. Geophys. Res.,* **106,** 17 237–17 252.

——, and Coauthors, 2005: Ice supersaturations exceeding 100% at the cold tropical tropopause: Implications for cirrus formation and dehydration. *Atmos. Chem. Phys.,* **5,** 851–862.

Johari, G. P., G. Fleissner, A. Hallbrucker, and E. Mayer, 1994: Thermodynamic continuity between glassy and normal water. *J. Phys. Chem.,* **98,** 4719–4725.

Kanno, H., M. Soga, and K. Kajiwara, 2007: Linear relation between T_H (homogeneous ice nucleation temperature) and T_m (melting temperature) for aqueous solutions of sucrose, trehalose, and maltose. *Chem. Phys. Lett.,* **443,** 280–283.

Kärcher, B., and U. Lohmann, 2002: A parameterization of cirrus cloud formation: Homogeneous freezing of supercooled aerosols. *J. Geophys. Res.,* **107,** 4010, doi:10.1029/2001JD000470.

——, and ——, 2003: A parameterization of cirrus cloud formation: Heterogeneous freezing. *J. Geophys. Res.,* **108,** 4402, doi:10.1029/2002JD003220.

——, J. Hendricks, and U. Lohmann, 2006: Physically based parameterization of cirrus cloud formation for use in global atmospheric models. *J. Geophys. Res.,* **111,** D01205, doi:10.1029/2005JD006219.

Kay, J. E., V. Tsemekhman, B. Larson, M. B. Baker, and B. D. Swanson, 2003: Comment on evidence for surface-initiated homogeneous nucleation. *Atmos. Chem. Phys.,* **3,** 1439–1443.

——, M. B. Baker, and D. Hegg, 2006: Microphysical and dynamical controls on cirrus cloud optical depth distributions. *J. Geophys. Res.,* **111,** D24205, doi:10.1029/2005JD006916.

Keith, D., 2000: Stratosphere-troposphere exchange: Inferences from the isotopic composition of water vapor. *J. Geophys. Res.,* **105,** 15 167–15 174.

Khalizov, A. F., M. E. Earle, W. J. W. Johnson, G. D. Stubley, and J. J. Sloan, 2006a: Development and characterization of a laminar aerosol flow tube. *Rev. Sci. Instrum.,* **77,** 033102, doi:10.1063/1.2175958.

——, ——, ——, ——, and ——, 2006b: Modeling of flow dynamics in laminar aerosol flow tubes. *J. Aerosol Sci.,* **37,** 1174–1187.

Khvorostyanov, V. I., and K. Sassen, 1998: Toward the theory of homogeneous nucleation and its parameterization for cloud models. *Geophys. Res. Lett.,* **25,** 3155–3158.

Khvorostyanov, V. I., and J. A. Curry, 2004: Thermodynamic theory of freezing and melting of water and aqueous solutions. *J. Phys. Chem.,* **108A,** 11 073–11 085.

Knopf, D. A., B. P. Luo, U. K. Krieger, and T. Koop, 2003: Thermodynamic dissociation constant of the bisulfate ion from raman and ion interaction modeling studies of aqueous sulfuric acid at low temperatures. *J. Phys. Chem.,* **107A,** 4322–4332.

——, ——, ——, and ——, 2005: Reply to ''Comment on the 'Thermodynamic dissociation constant of the bisulfate ion from raman and interaction modeling studies of aqueous sulfuric acid at low temperatures.'" *J. Phys. Chem.,* **109A,** 2707–2709.

Koop, T., 2004: Homogeneous ice nucleation in water and aqueous solutions. *Z. Phys. Chem.,* **218,** 1231–1258.

——, H. P. Ng, L. T. Molina, and M. J. Molina, 1998: A new optical technique to study aerosol phase transitions: The nucleation of ice from H_2SO_4 aerosols. *J. Phys. Chem.,* **102A,** 8924–8931.

——, B. Luo, A. Tsias, and T. Peter, 2000: Water activity as the determinant for homogeneous ice nucleation in aqueous solutions. *Nature,* **406,** 611–614.

Krämer, B., 1998: Freezing of single levitated micro-droplets of water, sulfuric acid and ternary $H_2SO_4/HNO_3/H_2O$ solutions. Ph.D. thesis, Frie University of Berlin, 184 pp.

Larson, B. H., 2004: Experimental investigations of ammonium sulfate-water solution droplet nucleation temperatures. M.S. thesis, ESS Department, University of Washington, 64 pp.

——, and B. D. Swanson, 2006: Experimental investigation of the homogeneous freezing of aqueous ammonium sulfate droplets. *J. Phys. Chem.,* **110A,** 1907–1916.

Mangold, A., R. Wagner, H. Saathoff, U. Schurath, C. Giesemann, B. Ebert, M. Krämer, and O. Möhler, 2005: Experimental investigation of ice nucleation by different types of aerosols in the aerosol chamber AIDA: Implications to microphysics of cirrus clouds. *Meteor. Z.,* **14,** 485–497.

Möhler, O., and Coauthors, 2003: Experimental investigation of homogeneous freezing of sulphuric acid particles in the aerosol chamber AIDA. *Atmos. Chem. Phys.,* **3,** 211–223.

Murphy, D. M., and T. Koop, 2005: Review of the vapour pressures of ice and supercooled water for atmospheric applications. *Quart. J. Roy. Meteor. Soc.,* **131,** 1539–1565.

Murray, B. J., D. A. Knopf, and A. K. Bertram, 2005: The formation of cubic ice under conditions relevant to earth's atmosphere. *Nature,* **434,** 202–205.

Peter, T., C. Marcolli, P. Spichtinger, T. Corti, M. B. Baker, and T. Koop, 2006: When dry air is too humid. *Science,* **314,** 1399–1402.

Prenni, A. J., P. J. DeMott, S. M. Kreidenweis, D. E. Sherman, L. M. Russell, and Y. Ming, 2001a: The effects of low molecular weight dicarboxylic acids on cloud formation. *J. Phys. Chem.,* **105A,** 11 240–11 248.

——, M. E. Wise, S. D. Brooks, and M. A. Tolbert, 2001b: Ice nucleation in sulfuric acid and ammonium sulfate particles. *J. Geophys. Res.,* **106,** 3037–3044.

Pruppacher, H. R., and J. D. Klett, 1997: *Microphysics of Clouds and Precipitation*. 2nd ed. Kluwer, 954 pp.

Rasmussen, D. H., and A. P. MacKinzie, 1972: Effect of solute on ice-solution interfacial free energy: Calculation from measured homogeneous nucleation temperatures. *Water Structure at the Water Polymer Interface,* H. H. G. Jellinek, Ed., Plenum Press, 126–145.

Sassen, K., and G. Dodd, 1988: Homogeneous nucleation rate for highly supercooled cirrus cloud droplets. *J. Atmos. Sci.,* **45,** 1357–1369.

Seeley, L. H., and G. T. Seidler, 2001: Two-dimensional nucleation of ice from supercooled water. *Phys. Rev. Lett.,* **87,** 055702, doi:10.1103/PhysRevLett.87.055702.

Shilling, J. E., T. J. Fortin, and M. A. Tolbert, 2006a: Depositional ice nucleation on crystalline organic and inorganic solids. *J. Geophys. Res.,* **111,** D12204, doi:10.1029/2005JD006664.

——, M. A. Tolbert, O. B. Toon, E. J. Jensen, B. J. Murray, and A. K. Bertram, 2006b: Measurements of the vapor pressure of cubic ice and their implications for atmospheric ice clouds. *Geophys. Res. Lett.,* **33,** L17801, doi:10.1029/2006GL026671.

Speedy, R. J., P. G. Debenedetti, R. S. Smith, C. Huang, and B. D. Kay, 1996: The evaporation rate, free energy, and entropy of amorphous water at 150 K. *J. Chem. Phys.,* **105,** 240–244.

Spichtinger, P., K. Gierens, and W. Read, 2002: The statistical distribution law of relative humidity in the global tropopause region. *Meteor. Z.,* **11,** 83–88.

Tabazadeh, A., E. J. Jensen, and O. B. Toon, 1997: A model description for cirrus cloud nucleation from homogeneous freezing of sulfate aerosols. *J. Geophys. Res.,* **102,** 23 845–23 850.

——, and Coauthors, 1998: Nitric acid scavenging by mineral and biomass burning aerosols. *Geophys. Res. Lett.,* **25,** 4185–4188.

——, Y. S. Djikaev, P. Hamill, and H. Reiss, 2002a: Laboratory evidence for surface nucleation of solid polar stratospheric cloud particles. *J. Phys. Chem. A,* **106,** 10 238–10 246.

——, ——, and H. Reiss, 2002b: Surface crystallization of supercooled water in clouds. *Proc. Natl. Acad. Sci. USA,* **99,** 15 873–15 878.

Treffeisen, R., R. Krejci, J. Ström, A. C. Engvaill, A. Herber, and L. Thomason, 2007: Humidity observations in the arctic troposphere over Ny-Ålesund, Svalbard based on 15 years of radiosonde data. *Atmos. Chem. Phys.,* **7,** 2721–2732.

Vortisch, H., B. Krämer, I. Weidinger, L. Wöste, T. Leisner, M. Schwell, H. Baumgärtel, and E. Rühl, 2000: Homogeneous freezing nucleation rates and crystallization dynamics of single levitated sulfuric acid solution droplets. *Phys. Chem. Chem. Phys.,* **2,** 1407–1413.

Wise, M. E., R. M. Garland, and M. A. Tolbert, 2004: Ice nucleation in internally mixed ammonium sulfate/dicarboxylic acid particles. *J. Geophys. Res.,* **109,** D19203, doi:10.1029/2003jd004313.

Wood, S. E., M. B. Baker, and B. D. Swanson, 2002: Instrument for studies of homogeneous and heterogeneous ice nucleation in free-falling supercooled water droplets. *Rev. Sci. Instrum.,* **73,** 3988–3996.

Zobrist, B., U. Weers, and T. Koop, 2003: Ice nucleation in aqueous solutions of poly[ethylene glycol] with different molar mass. *J. Chem. Phys.,* **118,** 10 254–10 261.

——, and Coauthors, 2006: Oxalic acid as a heterogeneous ice nucleus in the upper troposphere and its indirect aerosol effect. *Atmos. Chem. Phys.,* **6,** 3115–3129.

Zuberi, B., A. K. Bertram, T. Koop, L. T. Molina, and M. J. Molina, 2001: Heterogeneous freezing of aqueous particles induced by crystallized $(NH_4)_2SO_4$, ice, and letovicite. *J. Phys. Chem. A,* **105,** 6458–6464.